IEICE TRANS. ELECTRON., VOL.E87–C, NO.12 DECEMBER 2004

PAPER

A Resonant Slit-Type Probe for Millimeter-Wave Scanning Near-Field Microscopy

Tatsuo NOZOKIDO[†a)], ***Member***, **Tomohiro OHBAYASHI**[†], ***Nonmember***, **Jongsuck BAE**[†], ***Member***, ***and*** **Koji MIZUNO**[†], ***Fellow***

SUMMARY A resonant slit-type probe is proposed in this paper that can improve measurement sensitivity in millimeter-wave scanning near-field microscopy. The probe consists of a rectangular metal waveguide incorporating the following three sections; a straight section at the tip of the probe whose height is much smaller than the operating wavelength; a standard-height waveguide section; a quarter-wave transformer section to achieve impedance-matching between the other sections. The design procedure used for the probe is presented in detail and the performance of the fabricated resonant probe is evaluated experimentally. Experiments performed at U-band frequencies in which we reconstruct 2D images show that the sensitivity of the resonant probe is improved by more than four times compared with a conventional tapered slit-type probe. Some experimental results are compared with those obtained using the finite element method (Ansoft HFSS). Good agreement is demonstrated.

key words: *millimeter waves, scanning near-field microscopy, scanning probes, resonant slit-type probes, rectangular waveguides*

1. Introduction

The scanning near-field imaging technique has been utilized in a variety of instruments that cover frequencies spanning the microwave-to-optical regions. Many different kinds of near-field probes have been proposed and used during the development of this technique, because their design determines the image resolution and sensitivity attainable in scanning near-field microscopy [1]. Coaxial probes [2]–[6] are the most commonly used probe-type in the radio frequency regime, especially in the microwave region. The probes are made up of a fine coaxial cable with a sharpened central conductor protruding from the outer shielding. Spatial resolution is determined by the tip size of the inner conductor. A resolution of 50 nm has been reported for this kind of probe implemented in a commercial atomic force microscope (AFM) system at an operating frequency of 2.8 GHz [6]. Microstrip- and strip-lines, and a small aperture in a conducting screen have also been used as near-field probes in the microwave region [7]–[10]. A slit-type probe independently proposed by us [11], [12] and others [13]–[15] is suitable for use in the frequency region higher than the microwave regime because of the simplicity of its structure. The probe has a metal slit aperture that has a height much less than the operating wavelength λ, and a width of the order of λ at its apex. The slit probe can be operated in TE_{10} mode, and thus results in a high transmission efficiency because there is no cut-off effect. This high transmission characteristic leads to increased signal response with respect to variations in the physical parameters of objects to be imaged in scanning near-field microscopy, thus resulting in improved measurement sensitivity [1].

In this paper, we propose a new type of slit probe for use in millimeter-wave scanning near-field microscopy that can further improve measurement sensitivity. The probe incorporates a quarter-wave matching section inside the probe structure to increase transmission and to decrease reflection from the probe, thereby allowing high-sensitivity measurements. Since the matching section is constructed inside the probe, the probe itself is compact and there is no need for any additional tuning components, such as E-H tuners. The procedure that was used to design the probe is described in detail and the measured performance of the fabricated probe is reported.

2. Probe Structure and Design

Figure 1 shows our millimeter-wave microscope system using a slit-type probe. The probe incorporates a rectangular waveguide and has a slit aperture with dimensions of 4.8 mm in width ($w \sim \lambda$) $\times$ ~100 μm in height ($\ll \lambda$) at its apex. The system operates at U-band frequencies. Probe-to-object separation is maintained at 10 μm. The object to

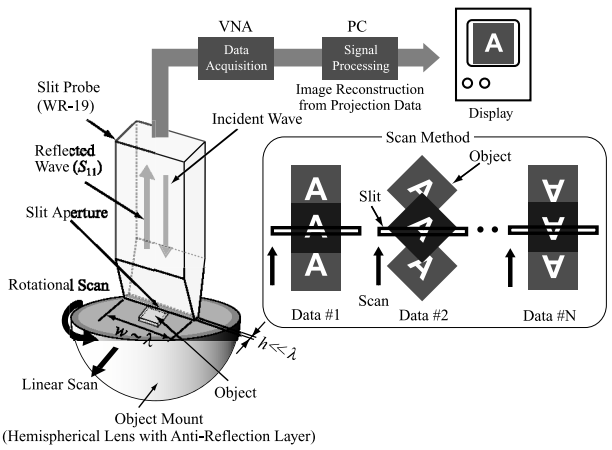

Fig. 1 Schematic of the experimental setup for millimeter-wave scanning near-field microscopy using a metal slit-type probe. The inset shows the scan method used during data acquisition.

Manuscript received May 19, 2004.
Manuscript revised August 12, 2004.

[†]The authors are with the Research Institute of Electrical Communication, Tohoku University, Sendai-shi, 980-8577 Japan.
a) E-mail: nozokido@riec.tohoku.ac.jp

be imaged is placed on an object mount consisting of a hemispherical glass lens and an anti-reflection (AR) layer to reduce unwanted signal fluctuations caused by surface waves in the object and reflection from the mount [16]. The glass lens and the AR layer are made from BK7 (a kind of borosilicate glass with a dielectric constant ε_r of 6.19) and polymethylmethacrylate (PMMA, ε_r = 2.56), respectively. The slit probe is connected to a vector network analyzer (VNA: HP85106) via waveguide-to-coaxial transformers to enable measurement of S_{11} signals, which are then reconstructed into 2D near-field images. We have adopted the scanning technique shown in the inset of Fig. 1 and additional signal processing in order to achieve sub-wavelength resolution in all directions [12]. As in computerized tomography, the target object is scanned linearly at different object-rotation angles using a scanner with stepper-motor-driven linear and rotational stages. The S_{11} signals acquired during these scans are then processed into images by an image-reconstruction code based on the filtered back-projection (FBP) method [17], which is the most commonly used image reconstruction technique in computerized tomography. A PC is used to control the VNA and the scanner, and also executes image reconstruction. All of the dielectric constants of the materials that appear in this paper were measured at U-band frequencies. In this measurement regime, a quasi-optical configuration was used to measure the transmission from material that had been processed into a parallel-plate shape as a function of frequency. The measured transmission data were fitted using *Fabry-Perot etalon* theory [18] and the best-fit parameters were taken as the dielectric constant.

Figure 2 compares the structure of a tapered slit-type probe that we have used in the past (a) with the resonant slit-type probe proposed in this paper (b). In both cases, the

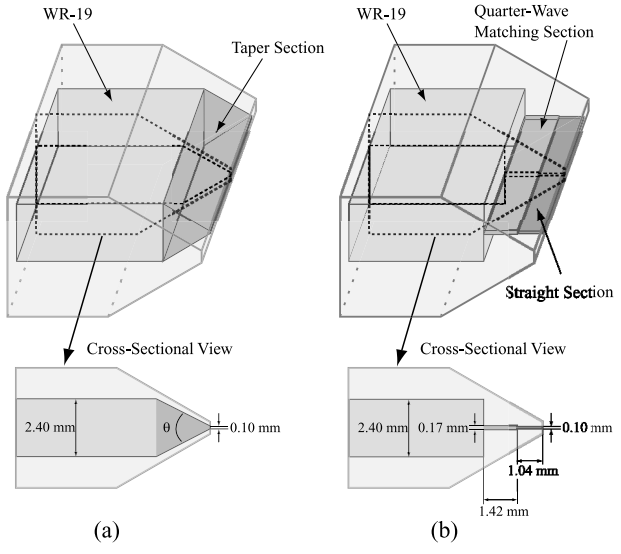

Fig. 2 Structures of the slit-type probes. (a) Tapered slit-type probe. (b) Resonant slit-type probe. The two lower figures show cross sections of each of the probes indicated with dotted lines in the upper figures.

waveguide width (4.8 mm) remains unchanged for all of the probes and the total waveguide length is 50 mm. In the case of the tapered probe, only the waveguide height is tapered linearly down to 100 μm, which is 1/50 of the wavelength at 60 GHz millimeter-wave frequency. The taper angle θ of the probe is 30 degrees. The resonant probe consists of the following three sections; a straight section at the tip of the probe, a standard-height waveguide (WR-19) section, and a quarter-wave transformer section to achieve impedance-matching between the other sections. The design procedure used for the resonant probe is as follows.

The resonant probe was designed to operate at a millimeter-wave frequency of 59 GHz, where the AR layer works most efficiently to reduce reflections [16]. The height of the straight section at the probe tip is assumed to be 100 μm. The length of the straight section L_{st} was initially determined using an Ansoft High-Frequency Structure Simulator (HFSS) ver. 8.0. The simulator was installed in a PC with a 2.0 GHz Pentium 4 processor and 2 GB of memory. All of the simulations using the HFSS that are discussed in this paper were executed using the E- and H-plane symmetries in order to reduce the amount of PC memory that was required. The convergence parameter, Max Delta S, was taken as 0.001. When obtaining S_{11} data as a function of frequency, the frequency was swept from 40 to 60 GHz in 0.1 GHz frequency steps after achieving this desired convergence of the solution at 59 GHz. Most of the simulations were completed in about 3 hours. The geometric model used in the HFSS simulation is described in Fig. 3. The model is surrounded by a radiation boundary, except for the input port. The object mount is modeled as a rectangular plate of BK7 with a thickness of 2 mm. A fused quartz plate (ε_r = 3.70) is taken as an object. Figure 4 shows how L_{st} was determined. As shown in Fig. 4(a), a model with only a straight section with a length of L_{pr} was simulated by HFSS to calculate S_{11}. The value of S_{11} at the probe tip (S_{11tip}) is calculated by

$$S_{11tip} = S_{11} \exp\left(2\gamma_{st} L_{pr}\right), \tag{1}$$

where γ_{st} is a propagation constant defined as [19]

$$\gamma_{st} = \alpha + j\beta, \tag{2}$$

$$\alpha = \frac{\sqrt{\pi\rho\mu_0 f}}{\eta_0 b_{st}} \frac{1}{\sqrt{1-\nu^2}} \left(1 + \frac{2b_{st}}{a}\nu^2\right), \tag{3}$$

$$\beta = \frac{2\pi}{\lambda_0}\sqrt{1-\nu^2}, \tag{4}$$

$$\nu = \frac{f_c}{f} = \frac{\lambda_0}{2a}. \tag{5}$$

Here, ρ, μ_0, f, η_0, a, b_{st}, f_c, and λ_0 are the resistivity of the probe metal ($2.44 \times 10^{-8}\,\Omega$·m for Au), the permeability in vacuum, the frequency of operation (59 GHz), the intrinsic impedance of free space (376.7 Ω), the waveguide width (4.8 mm), the waveguide height (100 μm), the cutoff frequency of the TE_{10} mode, and the wavelength in free space (5.08 mm), respectively. When L_{pr} is 7.5 mm, S_{11}

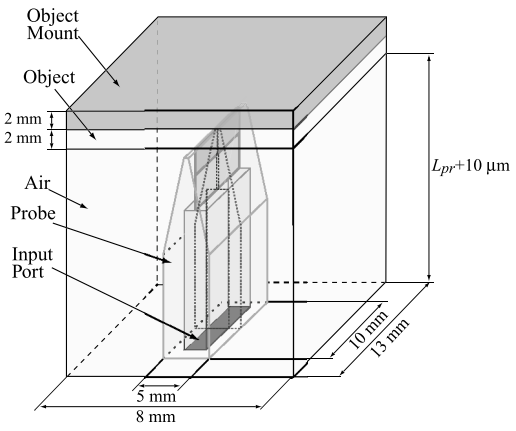

Fig. 3 Geometric model used in the HFSS simulation. In this figure, a resonant slit-type probe is placed in the model. The dimensions are not to scale.

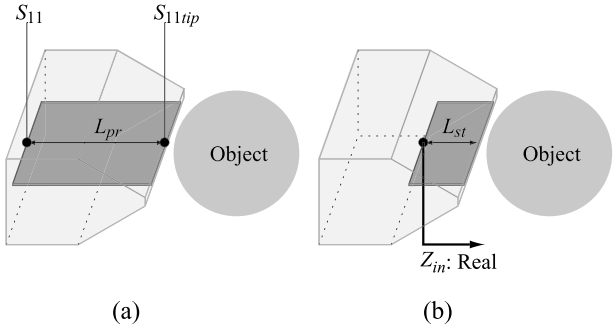

Fig. 4 Schematic drawing illustrating a method for determining the length of the straight section of the resonant slit-type probe. The value of S_{11} at the probe tip (S_{11tip}) is calculated by HFSS simulation (a), and then the length of the straight section L_{st} is determined in order to minimize the imaginary part of the input impedance Z_{in} observed from the left-hand end of the straight section (b).

was determined by HFSS simulation, as being $-0.506 + j0.579$. From the above equations, S_{11tip} was calculated to be $0.541 - j0.585$. The input impedance Z_{in} seen from the left-hand end of the straight section can be calculated using

$$Z_{in} = \frac{1 + S_{11tip}\exp(-2\gamma_{st}L_{st})}{1 - S_{11tip}\exp(-2\gamma_{st}L_{st})}Z_{st}, \tag{6}$$

where Z_{st} is the characteristic impedance of the straight section defined by [20]

$$Z_{st} = \frac{2\eta_0}{\sqrt{1-\nu^2}}\frac{b_{st}}{a}. \tag{7}$$

We have adopted this definition of the characteristic impedance because S_{11} signals (S parameters) are measured in this work and this notation is compatible with calculating S parameters in conventional equivalent circuit models for rectangular waveguides operated in TE_{10} mode. The length of the straight section L_{st} has been determined as 1.04 mm in order to minimize the imaginary part of Z_{in} (to within an accuracy of 10 μm, which is imposed by the possible errors in the actual manufacturing process of the probe). In this

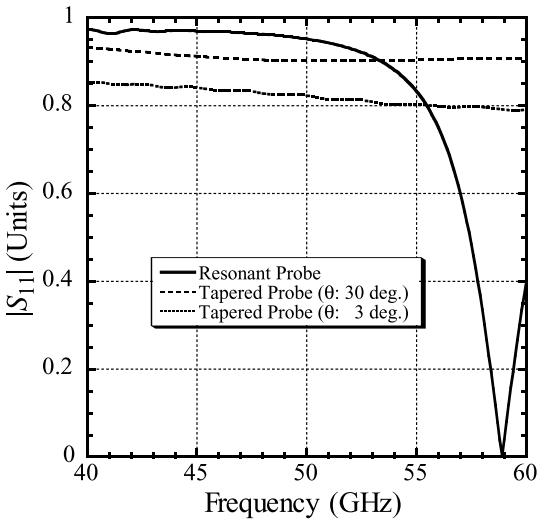

Fig. 5 $|S_{11}|$ calculated by HFSS as a function of frequency for the resonant probe design, and for tapered probes with taper angles θ of 30 degrees and of 3 degrees.

case, Z_{in} is estimated as $2.139 - j0.083\,\Omega \approx 2.139\,\Omega$.

The next step in the design is to determine the height b_{ms} and the length L_{ms} of the quarter-wave matching section. These can be calculated by using the following equations,

$$b_{ms} = a\frac{\sqrt{1-\nu^2}}{2\eta_0}\sqrt{Z_{in}Z_{WR}}, \tag{8}$$

$$L_{ms} = \frac{1}{4}\lambda_g = \frac{1}{4}\frac{\lambda_0}{\sqrt{1-\nu^2}}, \tag{9}$$

where Z_{WR} and λ_g are the characteristic impedance of the standard waveguide (WR-19) section (444.3 Ω) and the guide wavelength, respectively. Using Eqs. (8) and (9), with the same 10 μm accuracy condition, b_{ms} and L_{ms} were found to be 0.17 mm, and 1.50 mm, respectively. The value of $|S_{11}|$ calculated by HFSS as a function of frequency using the above parameters has revealed that the resonant frequency of the probe is 56.8 GHz. This is because the shunt capacitive susceptances [21] at each junction between the straight/matching sections and the matching/standard-height waveguide sections are not taken into account in Eq. (9). The length L_{ms} of the quarter-wave matching section was adjusted by HFSS simulation in order to make the probe resonant at the design frequency of 59 GHz, and the length L_{ms} has been determined as 1.42 mm, which is ∼5% smaller in value than that calculated using Eq. (9). The detailed dimensions of the waveguide for the resonant probe are depicted in Fig. 2(b).

Figure 5 shows values of $|S_{11}|$ as a function of frequency (calculated by HFSS) for the resonant probe designed above, and for tapered probes with taper angles θ of 30 degrees and 3 degrees. The second of these (30 degrees) is representative of the probe we used in the past, while the 3 degrees design has the minimum taper angle when the length of the probe is 50 mm. The value of $|S_{11}|$ of the resonant probe is almost zero at a frequency of 58.9 GHz, which is

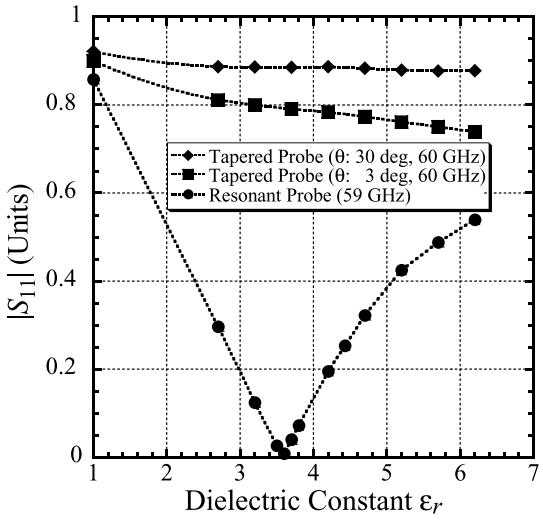

Fig. 6 $|S_{11}|$ calculated by HFSS as a function of the dielectric constant ε_r of the object.

very close to the design frequency of 59 GHz. The values of $|S_{11}|$ as calculated by HFSS as a function of the dielectric constant ε_r of the object for these three kinds of near-field probes are shown in Fig. 6. In this figure, the values of $|S_{11}|$ are plotted as a function of a dielectric constant ε_r of less than 6.19, since the dielectric constant of the object should be less than that of the material used for the hemispherical glass lens of the object mount in our microscope system in order to prevent unwanted signal fluctuations caused by surface waves within the object to be imaged [16]. The operating frequencies of the resonant probe and the tapered probes are 59 GHz and 60 GHz, respectively. Although the operating frequency of the tapered probes is different from that of the resonant probe, the same response is expected when the tapered probes are operated at 59 GHz (as shown in Fig. 5). It can be seen from Fig. 6 that the response of the resonant probe with respect to variations in the object dielectric constant is more than ten times higher than the response of the the tapered probe with a taper angle of 3 degrees. As shown in Figs. 5 and 6, the resonant probe is expected to operate with higher sensitivity than the tapered probes.

As described above, a resonant slit-probe has been designed at a millimeter-wave frequency of 59 GHz when a fused quartz plate (ε_r = 3.70) is taken as the target object. We have confirmed that this design procedure works well for an object dielectric constant ε_r of less than 6.19, which is the highest dielectric constant that can be imaged in our microscope system [16].

3. Experimental Results

A resonant probe was fabricated using an electro-forming technique. Figure 7 compares the measured value of $|S_{11}|$ and the value of $|S_{11}|$ calculated by HFSS of the fabricated resonant probe as a function of frequency when a fused quartz plate (a) and Pyrex glass (ε_r = 4.43) (b) were used as objects. Because the measured slit height (b_{st}) of the

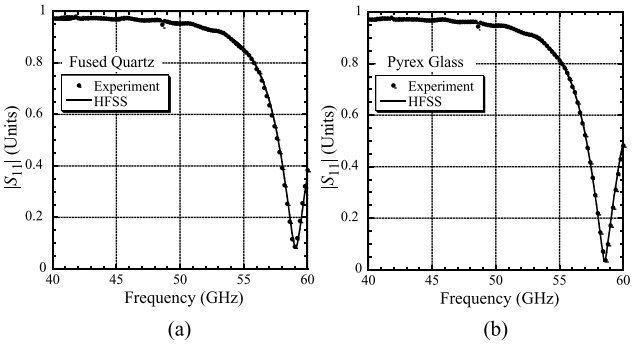

Fig. 7 Comparison of measured values of $|S_{11}|$ and values of $|S_{11}|$ calculated by HFSS for the fabricated resonant probe as a function of frequency when a fused quartz plate (a) and a Pyrex glass (b) are taken as objects.

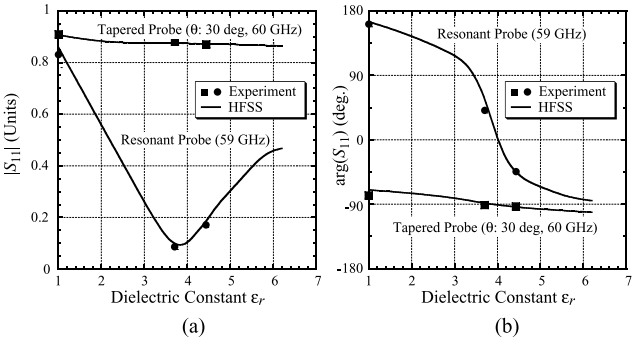

Fig. 8 Comparison of measured and calculated results of the magnitude (a) and the phase (b) of the reflection coefficient S_{11} as a function of the dielectric constant ε_r of the object for the resonant probe and the tapered probe with a taper angle of 30 degrees.

fabricated probe was 90 μm (which is 10 μm smaller than the design), this measured dimension was used in the HFSS simulation. The measured results agree quite well with the results calculated by HFSS. The same level of agreement is verified in Fig. 8, where the measured and the calculated results of the magnitude $|S_{11}|$ and also the phase $\arg(S_{11})$ of the reflection coefficient S_{11} as a function of the dielectric constant ε_r of the object are compared for the resonant probe and the probe with a taper angle of 30 degrees.

Raw data (projection data) sets for various 2D images were taken using the resonant probe and the tapered probe with a taper angle of 30 degrees. The target object was a metal patch deposited onto a quartz plate. Figure 9(a) shows an optical image of the object. The raw data were obtained under experimental conditions where the sampling interval for the linear scan, the sampling points for the linear scan, the sampling interval for the rotational scan, and the total number of projections were 40 μm, 100 points, 1.8 degrees, and 100, respectively. The data acquired through the scans were then processed into 2D intensity images by the FBP method. Figures 9(b) and (c) show reconstructed intensity images using the tapered probe and the resonant probe, respectively. The image size is 2800 μm $\times$ 2800 μm, and these images are displayed under the same conditions. It is obvious that the image reconstructed with the resonant probe

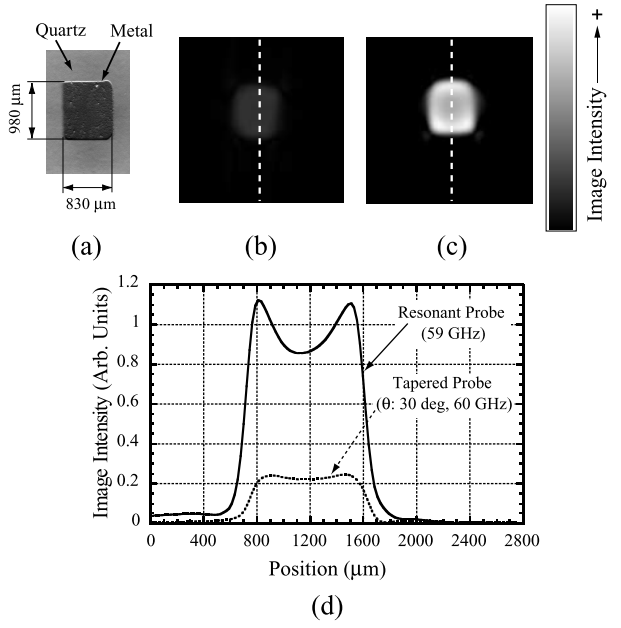

Fig. 9 Images of a metal patch. (a) Optical image. (b) Reconstructed intensity image using the tapered probe. (c) Reconstructed intensity image using the resonant probe. (d) One-dimensional intensity profiles along the dotted lines in (b) and (c).

is much brighter than that reconstructed with the tapered probe. Figure 9(d) shows one-dimensional intensity profiles along the dotted lines in Figs. 9(b) and (c). The image intensity is proportional to the absolute value of the vectorial difference between the reflected waves at each of the pixels and that at the quartz plate [12]. It can be seen from these profiles that the image intensity is enhanced by more than four times by using the resonant probe compared with the tapered probe. As described in our previous work [12], we tried to estimate the image resolution by differentiating the one-dimensional intensity profile acquired by the resonant probe in Fig. 9(d) to calculate the line-spread functions and found that an image resolution of $100\,\mu$m ($\sim \lambda/50$) had been achieved.

4. Conclusion

A resonant slit-type probe for use in millimeter-wave scanning near-field microscopy has been proposed, and its design procedure is described in detail. Reconstructed near-field images obtained at ~60 GHz show that the resonant probe proposed here has more than four times greater sensitivity than a tapered slit-type probe. It has been verified that HFSS can be used to simulate the interaction between the near-field probes and the objects to be imaged with a reasonable degree of accuracy.

The resonant probe proposed here allows high sensitivity measurements without any additional tuning components and may be useful for characterizing the uniformity of planar substrates for various millimeter-wave components with a sub-wavelength spatial resolution at the frequency of operation.

Acknowledgments

This work was supported in part by a Grant-In-Aid for Scientific Research, No. 15360181 from the Japan Society for the Promotion of Science (JSPS), the Support Center for Advanced Telecommunications Technology Research, Foundation (SCAT), Japan, and a Strategic Information and Communications R&D Promotion Programme (SCOPE) of the Ministry of Public Management, Home Affairs, Posts and Telecommunications (MPHPT), Japan.

References

[1] B.T. Rosner and D.W. van der Weide, "High-frequency near-field microscopy," Rev. Sci. Instrum., vol.73, no.7, pp.2505–2525, 2002.
[2] C. Gao, T. Wai, F. Duewer, Y. Lu, and X.-D. Xiang, "High spatial resolution quantitative microwave impedance microscopy by a scanning tip microwave near-field microscope," Appl. Phys. Lett., vol.70, no.13, pp.1872–1874, 1997.
[3] Y. Gao, A. lauer, Q. Ren, and I. Wolff, "Calibration of electric coaxial near-field probes and applications," IEEE Trans. Microw. Theory Tech., vol.46, no.11, pp.1694–1703, 1998.
[4] C.P. Vlahacos, D.E. Steinhauer, S.K. Dutta, B.J. Feenstra, S.M. Anlage, and F.C. Wellstood, "Quantitative topographic imaging using a near-field scanning microwave microscope," Appl. Phys. Lett., vol.72, no.14, pp.1778–1780, 1998.
[5] R. Kantor and I.V. Shvets, "Measurement of electric-field intensities using scanning near-field microwave microscopy," IEEE Trans. Microw. Theory Tech., vol.51, no.11, pp.2228–2234, 2003.
[6] M. Tabib-Azar and Y. Wang, "Design and fabrication of scanning near-field microwave probes compatible with atomic force microscopy to image embedded nanostructures," IEEE Trans. Microw. Theory Tech., vol.52, no.3, pp.971–979, 2004.
[7] M. Tabib-Azar, N.S. Shoemaker, and S. Harris, "Non-destructive characterization of materials by evanescent microwaves," Meas. Sci. Technol., vol.4, pp.583–590, 1993.
[8] M. Tabib-Azar. D.-P. Su, A. Pohar, S.R. LeClair, and G. Ponchak, "0.4 μm spatial resolution with 1 GHz (λ=30 cm) evanescent microwave probe," Rev. Sci. Instrum., vol.70. no.3, pp.1725–1729, 1999.
[9] E.A. Ash and G. Nicholls, "Super-resolution aperture scanning microscope," Nature, vol.237, pp.510–512, 1972.
[10] W.C. Symons, III, K.W. Whites, and R.A. Lodder, "Theoretical and experimental characterization of a near-field scanning microwave (NSMM)," IEEE Trans. Microw. Theory Tech., vol.51, no.1, pp.91–99, 2003.
[11] J. Bae, T. Okamoto, T. Fujii, K. Mizuno, and T. Nozokido, "Experimental demonstration for scanning near-field optical microscopy using a metal micro-slit probe at millimeter wavelengths," Appl. Phys. Lett., vol.71, no.24, pp.3581–3583. 1998.
[12] T. Nozokido, J. Bae, and K. Mizuno, "Scanning near-field millimeter-wave microscopy using a metal slit as a scanning probe," IEEE Trans. Microw. Theory Tech., vol.49, no.3, pp.491–499, 2001.
[13] S. Kawata, H. Takaoka, and Y. Inoue, "Slit-aperture SNOM for infrared spectroscopic micro-analysis," Conf. Digest of the NEAR FIELD OPTICS-3, EOS Topical Meeting, vol.8, pp.159–160, 1995.
[14] M. Golosovsky and D. Davidov, "Novel millimeter-wave near-field microscope," Appl. Phys. Lett., vol.68, no.11, pp.1579–1581, 1996.
[15] M. Golosovsky, A. Galkin, and D. Davidov, "High-spatial resolution resistivity mapping of large-area YBCO files by a near-field millimeter-wave microscope," IEEE Trans. Microw. Theory Tech., vol.44, no.7, pp.1390–1392, 1998.
[16] T. Nozokido, S. Nuimura, T. Hamano, J. Bae, and K. Mizuno,

"A new object mounting structure for use in millimeter-wave scanning near-field microscopy," IEICE Electronics Express, vol.1, no.6, pp.144–149, 2004.
[17] A.C. Kak and M. Slaney, Principles of computerized tomographic imaging, IEEE Press, New York, 1988.
[18] M. Born and E. Wolf, Principles of Optics (6th ed.), pp.323–367, pp.627–633, Pergamon Press, Oxford, 1991.
[19] R.E. Collin, Foundations for microwave engineering (2nd ed.), IEEE Press, New York, 1992.
[20] R.L. Eisenhart and P.J. Khan, "Theoretical and experimental analysis of a waveguide mounting structure," IEEE Trans. Microw. Theory Tech., vol.19, no.8, pp.706–719, 1971.
[21] R.F. Harrington, Time-harmonic electromagnetic fields, pp.171–177, McGraw-Hill, New York, 1961.

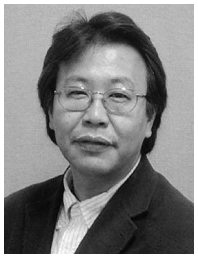

Tatsuo Nozokido received the B.Eng., M.Eng., and D.Eng. degrees in electrical engineering from Tohoku University in Sendai, Japan, in 1985, 1987, 1999, respectively. From 1987 to 1991, he was a Researcher at the Central Research Laboratory, Hitachi, Ltd., Tokyo, Japan. From 1991 to 1999, he was a Researcher at the Photodynamics Research Center, the Institute of Physical and Chemical Research (RIKEN), Sendai, Japan. From 1999 to 2000, he was with the Rutherford Appleton Laboratory (RAL), Oxon., U.K. He is currently Associate Professor at the Research Institute of Electrical Communication, Tohoku University, Sendai, Japan. His current research interests include millimeter and submillimeter-wave sources and imaging systems. Dr. Nozokido is a member of IEEE, and the Japan Society of Applied Physics.

Tomohiro Ohbayashi received the B.Eng. and M.Eng. degrees in electronic engineering from Tohoku University, Sendai, Japan in 2002 and 2004, respectively. He joined TOSHIBA Corporation in 2004. He is currently with Social Network & Infrastructure Systems Company, TOSHIBA Corporation.

Jongsuck Bae received the B.Eng. in electric engineering from the Korean University, Tokyo, in 1976. In 1977, he joined the Research Institute of Electrical Communication, Tohoku University, Sendai, Japan, where he was Associate Professor from 1992 to 2003. He received the D.Eng. degrees in electronic engineering from Tohoku University in 1990. He is currently Professor at Nagoya Institute of Technology, Nagoya, Japan. His research has been in developing quasi-optical components, such as oscillators, modulators, and couplers used for millimeter and submillimeter wavelengths, and their applications. Dr. Bae is a senior member of IEEE, and a member the Japan Society of Applied Physics.

Koji Mizuno graduated from the Department of Electronic Engineering, Tohoku University, Sendai, in 1963. He completed his Doctorate in Engineering in 1968. After being a research associate and an associate professor, he was appointed Professor (Research Institute of Electrical Communication) at the university in 1984. He was a visiting researcher at the University of London, London, in 1972, and at California Institute of Technology, Pasadena, in 1990. He concurrently served as a team leader at the Photodynamics Research Center, the Institute of Physical and Chemical Research (RIKEN), Sendai, from 1990–1998. During this time, he was involved in the research and development of devices and measuring instruments in the millimeter- and submillimeter-wave band. He received the IEEE Fellow grade in 1993, the Kenneth J. Button Medal in 1998, and the Minister Award of MEXT (Ministry of Education, Culture, Sports, Science and Technology, Japan) in 2003.